CHAPTER IV
RESULTS AND DISCUSSION

4.1 Photocatalyst Characterizations

4.1.1 TG-DTA Results

The TG-DTA curves were used to study the thermal decomposition behavior of the synthesized dried photocatalysts and to obtain their suitable calcination temperatures. Figure 4.1 exemplifies the TG-DTA curves of the dried pure TiO_2 and $0.05In_2O_3$-$0.95TiO_2$ gels. The DTA curves show three main exothermic regions. The first exothermic peak, with its position lower than 150 °C, is attributed to the removal of physisorbed water molecules. The second exothermic peak between 150 and 320 °C is attributed to the burnout of the LAHC surfactant molecules. The third exothermic region between 320 and 500 °C corresponds to the crystallization process of the photocatalysts and also the removal of organic remnants and chemisorbed water molecules (Hague *et al.*, 1994). The TG curves reveal that the calcination temperature of approximately 500 °C was sufficient for both the complete surfactant removal and the photocatalyst crystallization for both dried photocatalysts. Therefore, the calcination temperature in the range of 500 to 800 °C was used to investigate its effect on the physicochemical properties and the consequent photocatalytic CR dye degradation activity of all the synthesized photocatalysts.

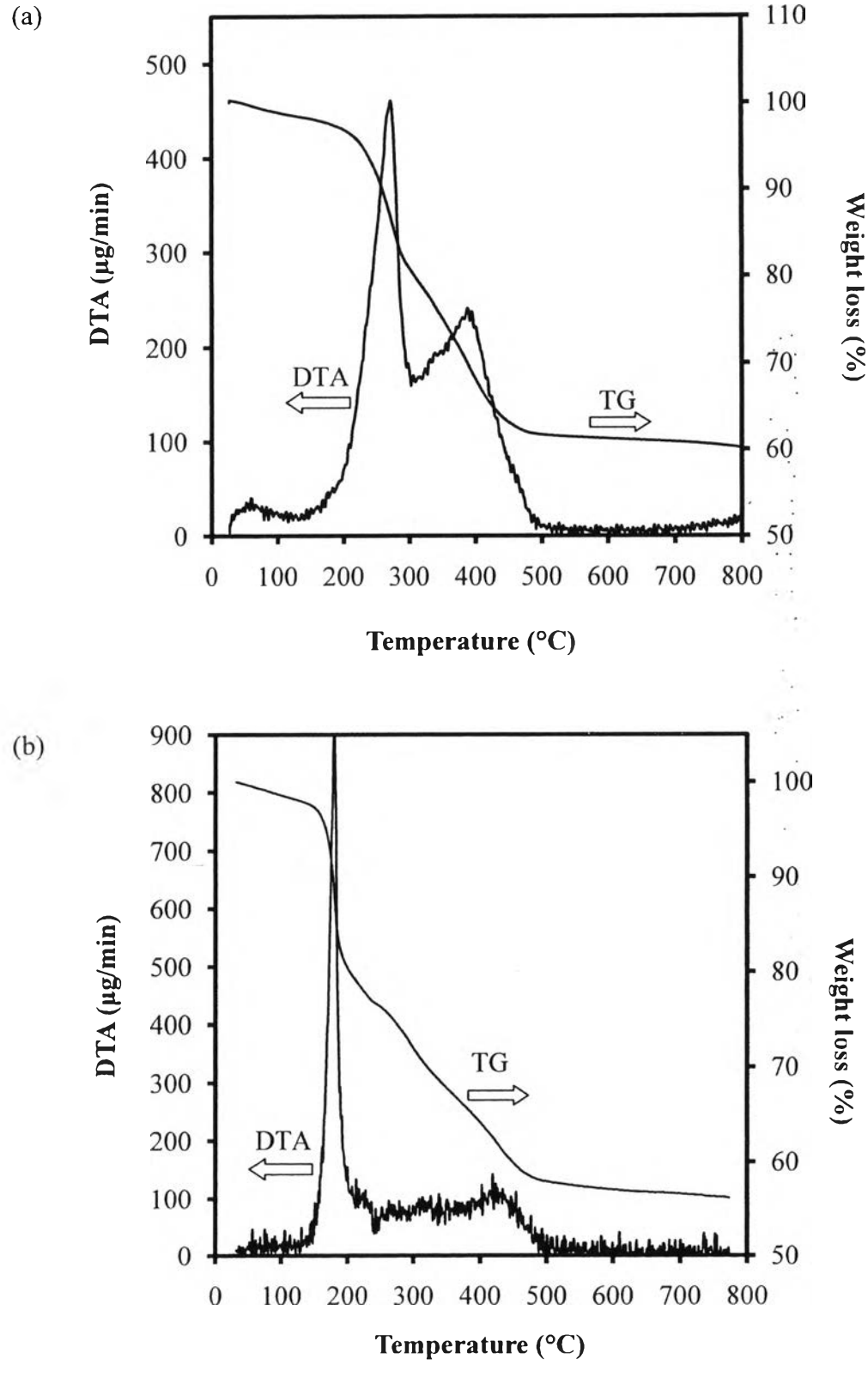

Figure 4.1 TG-DTA curves of the dried synthesized photocatalysts: (a) pure TiO_2 and (b) $0.05In_2O_3$-$0.95TiO_2$ mixed oxide.

4.1.2 N_2 Adsorption-Desorption Results

The N_2 adsorption-desorption analysis was used to verify the mesoporosity of the synthesized photocatalysts. The shape of the isotherms exhibits the characteristic behavior of the structure of powder, which is composed of an assembly of particles with uniform pore opening. The adsorption-desorption isotherms of the pure TiO_2, $0.05In_2O_3$-$0.95TiO_2$ mixed oxide (which provided the highest photocatalytic activity among the In_2O_3-TiO_2 mixed oxide series, as shown later), and 1.5 wt.% Ag-loaded $0.05In_2O_3$-$0.95TiO_2$ mixed oxide photocatalysts are exemplified in Figure 4.2. All of the samples exhibit a typical IUPAC type IV pattern with a hysteresis loop, which is the main characteristic of a mesoporous material (mesoporous size between 2 and 50 nm) according to the classification of IUPAC (Rouquerol *et al.*, 1999). A sharp increase in the adsorption curves at a high relative pressure (P/P_0) implies a capillary condensation of N_2 molecules inside the mesopores, implying the well-uniform mesopores and narrow pore size distributions since the P/P_0 position of the inflection point is directly related to the pore dimension. For the 1.5 wt.% Ag-loaded $0.05In_2O_3$-$0.95TiO_2$ mixed oxide photocatalyst, which provided the highest photocatalytic performance for CR dye degradation among the Ag-loaded $0.05In_2O_3$-$0.95TiO_2$ mixed oxide series as discussed later, its isotherms also exhibit the IUPAC type IV pattern. This implies that the Ag loading by the photochemical deposition (PCD) method did not significantly affect the mesoporous structure of the photocatalyst. Therefore, its mesoporous structure could be maintained. The insets of Figure 4.2 show the pore size distributions calculated from the desorption branch of the isotherms. All of the photocatalysts possess quite narrow pore size distributions entirely locating in the mesoporous region (between 2 and 50 nm), implying a good quality of the samples.

The textural properties, including specific surface area, mean mesopore diameter, and total pore volume, derived from the N_2 adsorption-desorption isotherms and pore size distributions of all the investigated In_2O_3-TiO_2 mixed oxide photocatalysts without and with Ag loading are summarized in Tables 4.1 and 4.2, respectively. For the synthesized mesoporous-assembled In_2O_3-TiO_2 mixed oxide photocatalysts calcined at a given temperature of 500 °C, the specific surface area, mean mesopore diameter, and total pore volume tended to increase with

increasing In_2O_3 content. Moreover, the mesoporous-assembled $0.05In_2O_3$-$0.95TiO_2$ mixed oxide photocatalyst was selected to further investigate the effect of calcination temperature in the range of 500 to 800 °C, as compared to the mesoporous-assembled pure TiO_2 photocatalyst, since it exhibited the highest photocatalytic activity, as mentioned above and shown later. With increasing calcination temperature from 500 to 800 °C, it can be seen that the $0.05In_2O_3$-$0.95TiO_2$ mixed oxide photocatalyst possessed a lower specific surface area; however, it could retain its specific surface area better than the pure TiO_2 photocatalyst at all identical calcination temperatures. The specific surface area of the pure TiO_2 decreased more quickly from 55.9 to 1.9 $m^2 \cdot g^{-1}$ as compared to the $0.05In_2O_3$-$0.95TiO_2$ mixed oxide, of which the specific surface area decreased from 88.3 to 19.9 $m^2 \cdot g^{-1}$ when increasing calcination temperature from 500 to 800 °C. The observed loss in the specific surface area with increasing calcination temperature is possibly because of the pore coalescence due to the crystallization of walls separating mesopores. These tendency also caused an increase in the mean mesopore diameter of photocatalysts, which still located in a narrow range between 5 and 17 nm, as well as a decrease in their total pore volume. For the case of Ag-loaded mesoporous-assembled $0.05In_2O_3$-$0.95TiO_2$ mixed oxide photocatalysts calcined at 500 °C (Table 4.2), it was found that an increase in the Ag loading led to a slight increase in the specific surface area. However, it did not significantly change the mean mesopore diameter and total pore volume due to its low loadings in the investigated range of 0-2 wt.%.

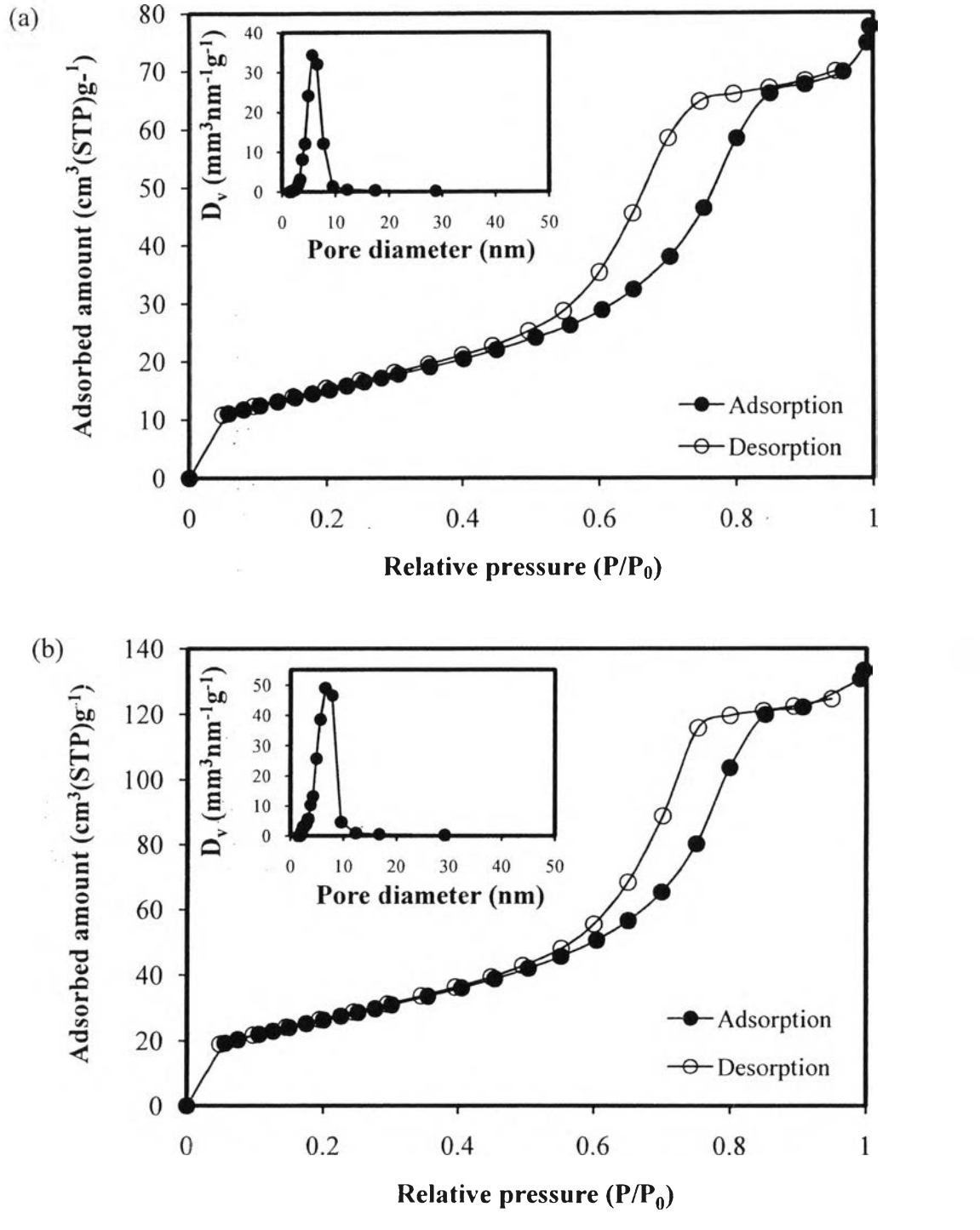

Figure 4.2 N_2 adsorption-desorption isotherms and pore size distributions (inset) of the synthesized mesoporous-assembled photocatalyst calcined at 500 °C: (a) pure TiO_2, (b) $0.05In_2O_3$-$0.95TiO_2$ mixed oxide, and (c) 1.5 wt.% Ag-loaded $0.05In_2O_3$-$0.95TiO_2$ mixed oxide.

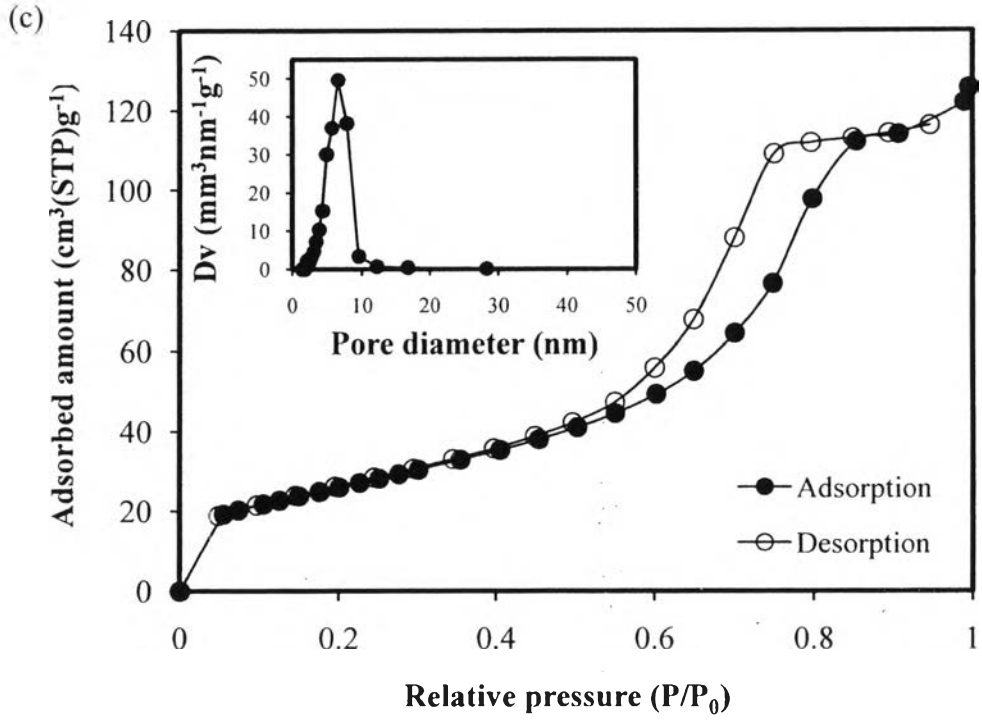

Figure 4.2 (Continued) N_2 adsorption-desorption isotherms and pore size distributions (inset) of the synthesized mesoporous-assembled photocatalyst calcined at 500°C: (a) pure TiO_2, (b) $0.05In_2O_3$-$0.95TiO_2$ mixed oxide, and (c) 1.5 wt.% Ag-loaded $0.05In_2O_3$-$0.95TiO_2$ mixed oxide.

Table 4.1 N_2 adsorption-desorption results of the synthesized mesoporous-assembled pure TiO_2 and In_2O_3-TiO_2 mixed oxide photocatalysts calcined at various temperatures

Photocatalyst	Calcination temperature (°C)	Specific surface area (m^2g^{-1})	Mean mesopore diameter (nm)	Total pore volume (cm^3g^{-1})
Pure TiO_2	500	55.9	5.61	0.115
$0.03In_2O_3$-$0.97TiO_2$	500	100.9	6.57	0.192
$0.05In_2O_3$-$0.95TiO_2$	500	88.3	7.83	0.196
$0.07In_2O_3$-$0.93TiO_2$	500	101.9	7.86	0.238
Pure TiO_2	500	55.9	5.61	0.115
	600	17.3	4.29	0.041
	700	4.1	-[a]	-[a]
	800	1.9	-[a]	-[a]
$0.05In_2O_3$-$0.95TiO_2$	500	88.3	7.83	0.196
	600	69.8	9.66	0.202
	700	61.0	12.41	0.203
	800	19.9	17.43	0.118

[(a)] N_2 adsorption-desorption isotherms correspond to IUPAC type II pattern.

Table 4.2 N_2 adsorption-desorption results of the synthesized Ag-loaded mesoporous-assembled $0.05In_2O_3$-$0.95TiO_2$ mixed oxide photocatalysts calcined at 500 °C

Ag loading (wt.%)	Specific surface area (m^2g^{-1})	Mean mesopore diameter (nm)	Total pore volume (cm^3g^{-1})
0	88.3	7.83	0.196
0.5	90.8	6.53	0.184
1	93.9	6.60	0.185
1.25	95.5	6.55	0.189
1.5	106.0	6.57	0.212
1.75	108.0	7.76	0.212
2	104.0	6.55	0.204

4.1.3 XRD Results

The XRD analysis was used to identify the crystalline phases of the synthesized photocatalysts. The XRD patterns of the synthesized mesoporous-assembled In_2O_3-TiO_2 mixed oxide photocatalysts with different In_2O_3-to-TiO_2 molar ratios calcined at 500 °C, as compared to the mesoporous-assembled pure TiO_2 photocatalyst, are shown in Figure 4.3. The XRD patterns of all samples show crystalline structure of the pure TiO_2 anatase phase. The dominant peaks at 2θ of about 25.4°, 37.9°, 48.2°, 54.0° and 55.2°, which represent the indices of (101), (004), (200), (105), and (211) planes, respectively, correspond to the anatase TiO_2 phase (JCPDS Card No. 21-1272) (Smith, 1960). However, it can be observed that the peak intensities progressively decreased with increasing In_2O_3 content possibly because a further increase in the In_2O_3 content retards the crystallization process of the TiO_2. Figure 4.4 comparatively shows the XRD patterns of the mesoporous-assembled pure TiO_2 and $0.05In_2O_3$-$0.95TiO_2$ mixed oxide photocatalysts calcined at various

temperatures between 500 and 800 °C. From Figure 4.4(a), the XRD pattern of the pure TiO_2 calcined at 500 °C shows crystalline structure of the pure anatase phase, as mentioned above. The pure TiO_2 sample underwent a phase transformation from the anatase to rutile phase beginning at 600 °C, resulting in the combination of the anatase and rutile phases. The occurrence of the dominant peaks at 2θ of about 27.6°, 36.2°, 41.4°, 44.2°, 54.3°, and 56.7°,which correspond to the indices of (110), (101), (111), (210), (211), and (220) planes, respectively, indicates the presence of the rutile TiO_2 phase (JCPDS Card No. 21-1276) (Smith, 1960). A steadily increased transformation was observed until the pure TiO_2 contained almost the pure rutile phase after being calcined at 800 °C. However, this phase transformation behavior was not observed for the $0.05In_2O_3$-$0.95TiO_2$ mixed oxide until the calcination temperature up to 800 °C, as shown in Figure 4.4(b). When the $0.05In_2O_3$-$0.95TiO_2$ mixed oxide photocatalyst was calcined at different temperatures, the anatase TiO_2 was still the major crystalline phase. This indicates its higher thermal stability as compared to the pure TiO_2. In addition, there were the peaks appearing at 2θ of 30.9° and 32.6° at the calcination temperature of 800 °C. These peaks correspond to the indices of (104) and (110) planes of the rhombic In_2O_3 phase (JCPDS Card No. 22-0336) (Smith, 1960), respectively. These results indicate that the incorporation of In_2O_3 could delay the anatase-to-rutile TiO_2 phase transformation until the calcination temperature reached as high as 800 °C, at which the separation of In_2O_3 phase was clearly observed. This implies that as long as the In_2O_3 phase was not significantly separated from the In_2O_3-TiO_2 mixed oxide, the anatase TiO_2 phase could be maintained at a given more severe calcination temperature, without transforming to the rutile TiO_2 phase. Figure 4.5 shows the XRD patterns of the synthesized Ag-loaded mesoporous-assembled $0.05In_2O_3$-$0.95TiO_2$ mixed oxide photocatalysts calcined at 500 °C. It can be seen that all the dominant peaks belonged to the anatase TiO_2 phase. It could be interestingly found that the Ag loadings higher than 1.5 wt.% by the PCD method partially induced an appearance of the rhombic In_2O_3 phase. This may be hypothesized that the coexisted In_2O_3 phase was forced to dominantly separate during this process. In addition, at the Ag loading higher than 0.5 wt.%, the presence of the Ag phase was observed due to the dominant peak of metallic silver at 2θ of 28°, which corresponds to the index of (110)

plane of the face-centered cubic Ag phase (JCPDS Card No. 22-0336)) (Smith, 1960).

The crystallite sizes of all the synthesized photocatalysts were estimated from the line broadening of the correlative X-ray diffraction peak of each crystalline phase by using the Scherrer equation (Cullity, 1978) (Eq. 4.1):

$$L = \frac{k\lambda}{\beta \cos(\theta)} \tag{4.1}$$

where L is the crystallite size, k is the Sherrer constant usually taken as 0.89, λ is the wavelength of the X-ray radiation (0.15418 nm for Cu Kα), β is the full width at half maximum (FWHM) of the diffraction peak measured at 2θ, and θ is the diffraction angle. The summary of XRD results of all investigated photocatalysts without and with Ag loading are summarized in Tables 4.3 and 4.4, respectively. The crystallite size of the In_2O_3-TiO_2 mixed oxide samples decreased from 10.56 to 6.62 nm with increasing In_2O_3 content, indicating the role of In_2O_3 in retarding the TiO_2 crystallization. In addition, it was observed that the crystallite size of the $0.05In_2O_3$-$0.95TiO_2$ mixed oxide photocatalyst moderately increased from 6.92 to 18.16 nm (anatase) and 19.05 nm (rutile) as the calcination temperature increased from 500 to 800 °C, whereas that of the pure TiO_2 photocatalyst remarkably increased from 10.56 to 29.63 nm (anatase) and 37.66 nm (retule). This is due to the fact that a higher calcination temperature resulted in the growth and sintering of small particles. For the Ag loaded $0.05In_2O_3$-$0.95TiO_2$ mixed oxide photocatalysts calcined at 500 °C, the results show that the Ag loading in the investigated range of 0-2 wt.% did not significantly affect the crystallite size of the TiO_2, whereas the increase in Ag loading led to increase in crystallite size of the In_2O_3. This may be possibly due to the influence of a higher content of the loaded Ag to more significantly induce the separation and growth of the In_2O_3 crystallite.

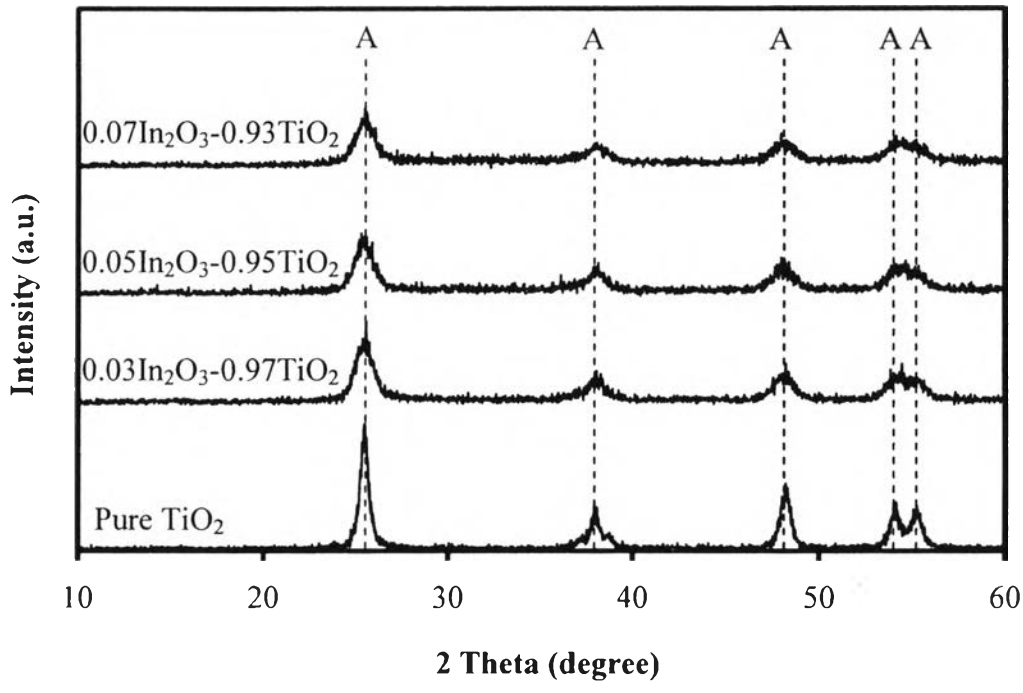

Figure 4.3 XRD patterns of the synthesized mesoporous-assembled In_2O_3-TiO_2 mixed oxide photocatalysts calcined at 500 °C (A = Anatase TiO_2).

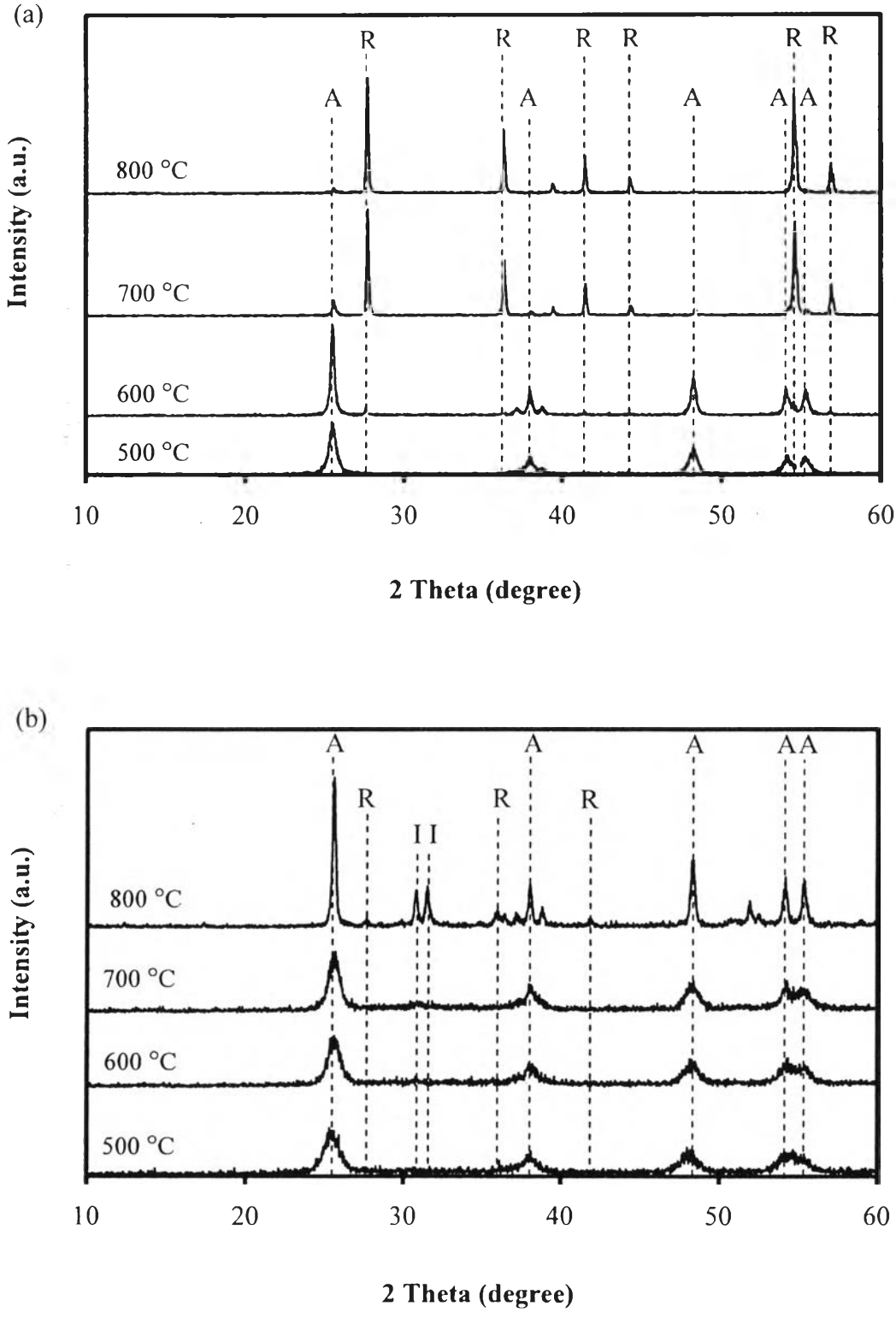

Figure 4.4 XRD patterns of the synthesized mesoporous-assembled photocatalysts calcined at various temperatures: (a) pure TiO_2 and (b) $0.05In_2O_3$-$0.95TiO_2$ mixed oxide (A = Anatase TiO_2, R = Rutile TiO_2, I = Rhombic In_2O_3).

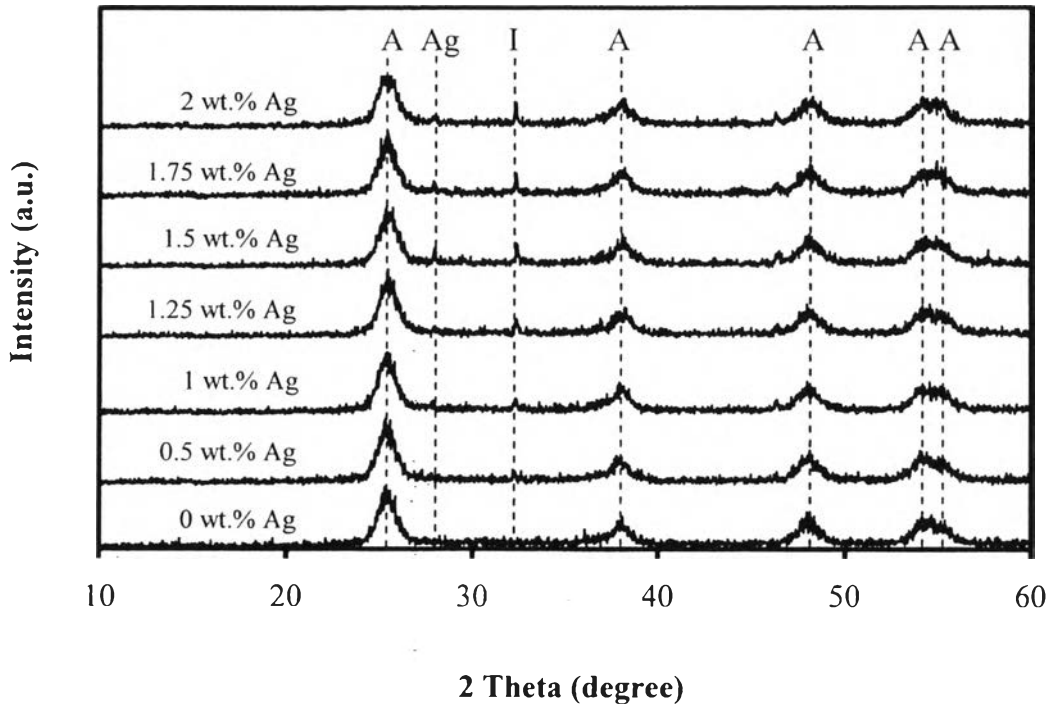

Figure 4.5 XRD patterns of the synthesized Ag-loaded mesoporous-assembled $0.05In_2O_3$-$0.95TiO_2$ mixed oxide photocatalysts calcined at 500 °C (A = Anatase TiO_2, I = Rhombic In_2O_3, Ag = Cubic Ag).

Table 4.3 XRD results of the synthesized mesoporous-assembled TiO_2 and In_2O_3-TiO_2 mixed oxide photocatalysts calcined at various temperatures

Photocatalyst	Calcination Temperature (°C)	Phase from XRD pattern	Rutile ratio	Crystallite size (nm)		
				Anatase TiO_2	Rutile TiO_2	Rhombic In_2O_3
Pure TiO_2	500	Anatase	-	10.56	-	-
$0.03In_2O_3$-$0.97TiO_2$	500	Anatase	-	7.03	-	-
$0.05In_2O_3$-$0.95TiO_2$	500	Anatase	-	6.92	-	-
$0.07In_2O_3$-$0.93TiO_2$	500	Anatase	-	6.62	-	-
Pure TiO_2	500	Anatase	-	10.56	-	-
	600	Anatase + Rutile	9.62	13.92	14.10	-
	700	Anatase + Rutile	89.58	29.32	30.90	-
	800	Anatase + Rutile	96.38	29.63	37.66	-
$0.05In_2O_3$-$0.95TiO_2$	500	Anatase	-	6.92	-	-
	600	Anatase	-	8.10	-	-
	700	Anatase	-	8.74	-	-
	800	Anatase + Rutile + Rhombic	5.30	18.16	19.05	29.79

Table 4.4 XRD results of the synthesized Ag-loaded mesoporous-assembled $0.05In_2O_3$-$0.95TiO_2$ mixed oxide photocatalysts calcined 500 °C

Ag loading content (wt.%)	Phase from XRD pattern	Crystallite size (nm)	
		Anatase TiO_2	Rhombic In_2O_3
0	Anatase	6.92	-
0.5	Anatase + Rhombic	6.84	14.88
1		7.57	22.74
1.25		6.81	23.39
1.5		6.56	30.32
1.75		7.93	32.75
2		6.46	40.95

4.1.4 UV-Visible Spectroscopy Results

UV-visible spectroscopy was used to examine the light absorption ability of all synthesized photocatalysts. The UV-visible spectra of the mesoporous-assembled In_2O_3-TiO_2 mixed oxide photocatalysts with different In_2O_3-to-TiO_2 molar ratios calcined at 500 °C, mesoporous-assembled pure TiO_2 photocatalyst calcined at 500-800 °C, mesoporous-assembled $0.05In_2O_3$-$0.95TiO_2$ mixed oxide photocatalyst calcined at 500-800 °C, and Ag-loaded mesoporous-assembled $0.05In_2O_3$-$0.95TiO_2$ mixed oxide photocatalysts calcined at 500 °C are comparatively shown in Figure 4.6. The results of absorption onset wavelength and corresponding band gap energy of all photocatalysts without and with Ag loading are summarized in Tables 4.5 and 4.6, respectively. It was observed that the absorption band of the synthesized mesoporous-assembled In_2O_3-TiO_2 mixed oxide photocatalysts was mainly in the UV light range of less than 400 nm (Figure 4.6(a)), and the absorption onset wavelength shifted to a shorter value with increasing In_2O_3 content (Table 4.5). From Table 4.5, the band gap energy (E_g, eV) of the mesoporous-assembled In_2O_3-TiO_2 mixed oxide photocatalysts therefore gradually increased in the range of 3.20 to 3.31 eV, which

was obtained from extrapolating the absorption onset of the rising part to x-axis (λ_g, nm) of the plots, as shown by dotted lines in Figure 4.6(a), and calculating by Eq. (4.2).

$$E_g = \frac{1240}{\lambda_g} \tag{4.2}$$

where λ_g is the absorption onset wavelength (nm) of the exciting light. In case of increasing calcination temperature from 500 to 800 °C of the mesoporous-assembled pure TiO_2 and $0.05In_2O_3$-$0.95TiO_2$ mixed oxide photocatalysts, as shown in Figures 4.6(b) and 4.6(c), respectively, the shift of the absorption onset edges toward a longer wavelength with an increase in the calcination temperature was observed only in the pure TiO_2 photocatalyst (Figure 4.6(b)). This shift is normally due to the narrowing of the band gap energy, which results in a lower energy required for electron to be excited from the valence band to conduction band (Sreethawong *et al.*, 2009). The absorption onset was approximately at 387 nm for the mesoporous-assembled pure TiO_2 photocatalyst calcined at 500 °C (Table 4.5), which corresponds to the band gap energy of the anatase TiO_2 of 3.20 eV. For the mesoporous-assembled pure TiO_2 photocatalyst calcined at 600 °C, the absorption onset shifted to the wavelength of 400 nm, which is correlated to the band gap energy of the mixed rutile and anatase TiO_2 between 3.02 and 3.20 eV, whereas the absorption onset of the mesoporous-assembled pure TiO_2 photocatalyst calcined at 700 and 800 °C further shifted to the wavelength of approximately longer 410 nm, which is correlated to the band gap energy of the rutile TiO_2. Their band gap energies reported corresponds very well to their crystalline phases obtained from the XRD analysis (Figure 4.4(a)). In contrast, the band gap energy of the mesoporous-assembled $0.05In_2O_3$-$0.95TiO_2$ mixed oxide photocatalyst was maintained approximately at the anatase TiO_2 band gap energy, even though it was calcined at as high as 800 °C, indicating its higher thermal stability compared to the pure TiO_2 photocatalyst, as mentioned above. These results confirm that the incorporation of In_2O_3 can inhibit the phase transformation of TiO_2 from the anatase to rutile phase. Moreover, the UV-visible spectra of the mesoporous-assembled $0.05In_2O_3$-$0.95TiO_2$ mixed oxide photocatalysts without and with 1.5 wt.% Ag loading calcined at 500 °C are exemplified in Figure 4.6(d). It can be seen that the absorption onset wavelength of the mesoporous-assembled

$0.05In_2O_3$-$0.95TiO_2$ mixed oxide photocatalyst slightly shifted to a shorter value with the Ag loading. The band gap energy of the Ag-loaded mesoporous-assembled $0.05In_2O_3$-$0.95TiO_2$ mixed oxide photocatalysts was in the range of 3.32-3.41 eV (λ_g ~ 364-374 nm) as compared to 3.30 eV (λ_g ~ 376 nm) of the unloaded mixed oxide photocatalyst (Table 4.6). In addition, it was clearly observed that the Ag-loaded mixed oxide photocatalysts showed more visible light absorption ability than the unloaded mixed oxide photocatalyst; however, this is not considered to be the main focus since the light source used for the photocatalytic activity tests emitted mostly UV light (λ < 400 nm).

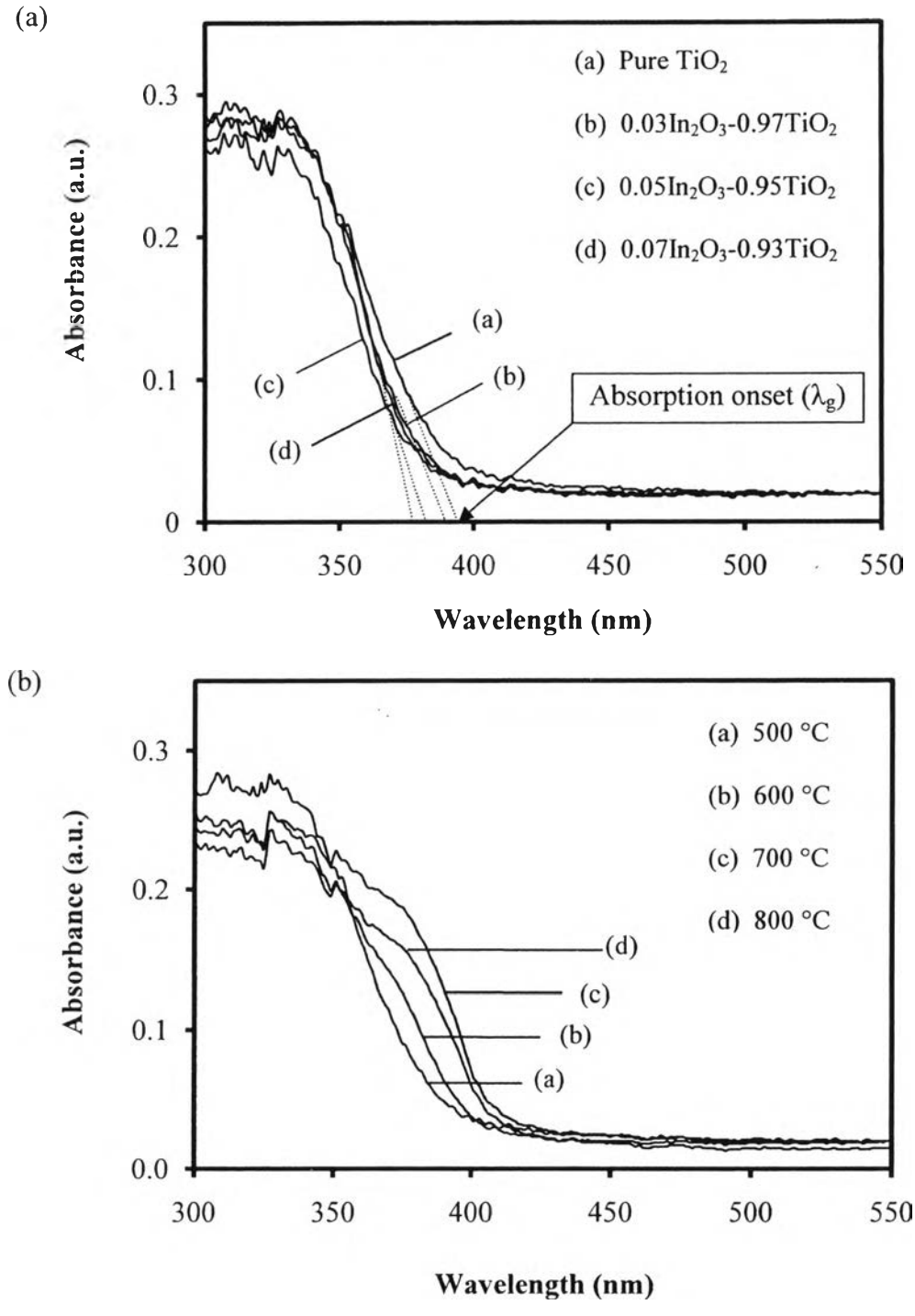

Figure 4.6 UV-visible spectra of the synthesized mesoporous-assembled photocatalysts: (a) pure TiO_2 and In_2O_3-TiO_2 mixed oxide calcined at 500 °C, (b) pure TiO_2 calcined at 500-800 °C, (c) $0.05In_2O_3$-$0.95TiO_2$ mixed oxide calcined at 500-800 °C, and (d) $0.05In_2O_3$-$0.95TiO_2$ mixed oxide without and with 1.5 wt.% Ag loading calcined at 500 °C.

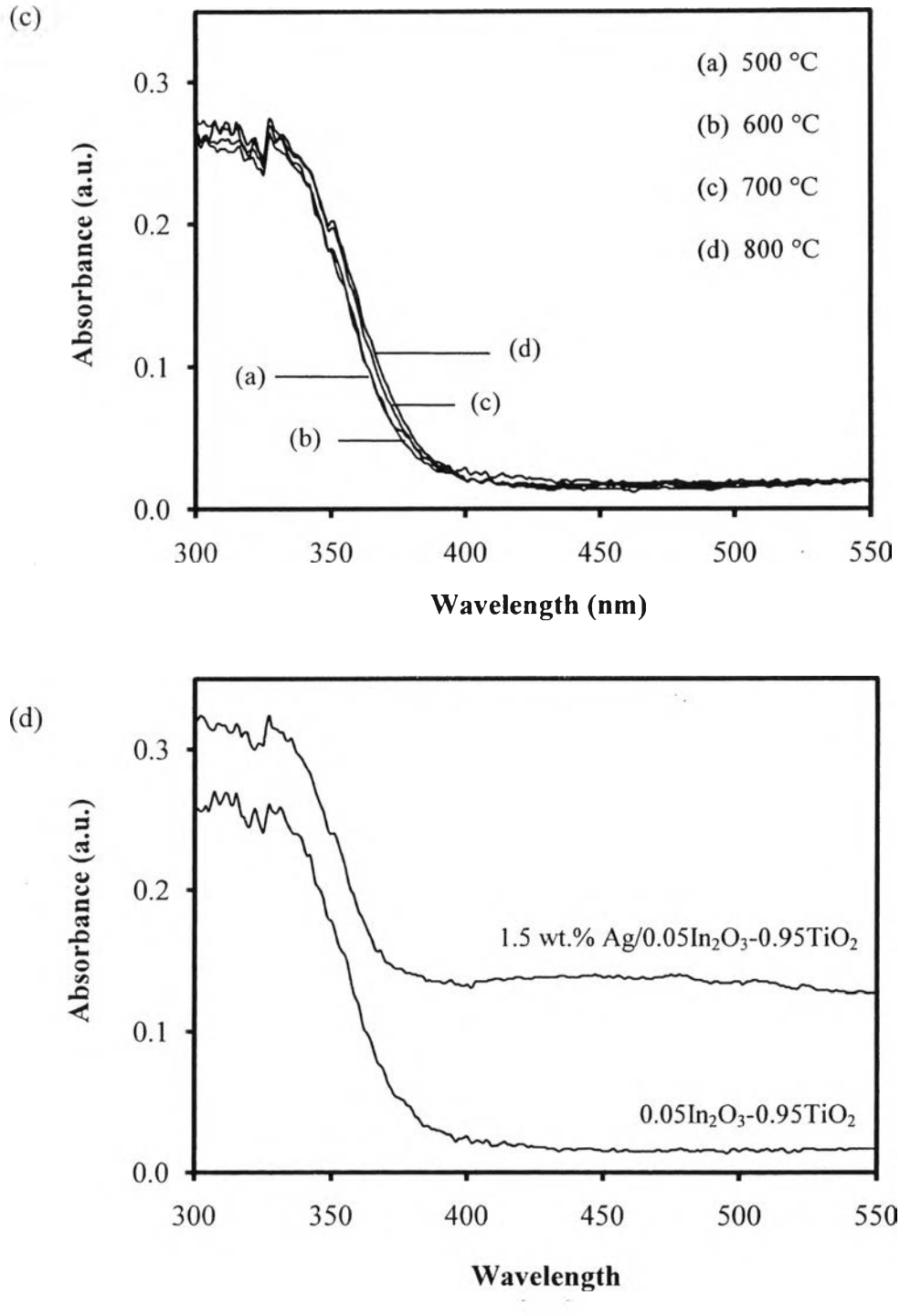

Figure 4.6 (Continued) UV-visible spectra of the synthesized mesoporous-assembled photocatalysts: (a) pure TiO_2 and In_2O_3-TiO_2 mixed oxide calcined at 500 °C, (b) pure TiO_2 calcined at 500-800 °C, (c) $0.05In_2O_3$-$0.95TiO_2$ mixed oxide calcined at 500-800 °C, and (d) $0.05In_2O_3$-$0.95TiO_2$ mixed oxide without and with 1.5 wt.% Ag loading calcined at 500 °C.

Table 4.5 Absorption onset wavelength and band gap energy results of the synthesized mesoporous-assembled pure TiO_2 and In_2O_3-TiO_2 mixed oxide photocatalysts calcined at various temperatures

Photocatalyst	Calcination temperature (°C)	Absorption onset wavelength, λ_g (nm)	Band gap energy (eV)
Pure TiO_2	500	387	3.20
$0.03In_2O_3$-$0.97TiO_2$	500	380	3.26
$0.05In_2O_3$-$0.95TiO_2$	500	376	3.30
$0.07In_2O_3$-$0.93TiO_2$	500	375	3.31
Pure TiO_2	500	387	3.20
	600	400	3.10
	700	410	3.02
	800	412	3.01
$0.05In_2O_3$-$0.95TiO_2$	500	376	3.30
	600	378	3.28
	700	380	3.26
	800	382	3.25

Table 4.6 Absorption onset wavelength and band gap energy results of the synthesized Ag-loaded mesoporous-assembled $0.05In_2O_3$-$0.95TiO_2$ mixed oxide photocatalysts calcined at 500 °C

Ag loading (wt.%)	Absorption onset wavelength λ_g (nm)	Band gap energy (eV)
0	376	3.30
0.5	374	3.32
1	373	3.32
1.25	370	3.35
1.5	368	3.37
1.75	366	3.39
2	364	3.41

4.1.5 SEM-EDX Results

The SEM images of the synthesized $0.05In_2O_3$-$0.95TiO_2$ and 1.5 wt.% Ag-loaded $0.05In_2O_3$-$0.95TiO_2$ mixed oxide photocatalysts are shown in Figures 4.7(a) and 4.8(a), respectively. The SEM images show the quite uniform-size particles of the samples in the form of aggregated clusters consisting of many nanoparticles. This nanoparticle aggregation can be possibly the cause of the mesoporous-assembled structure formation in the synthesized photocatalysts. The elemental distribution of the samples was investigated by the EDX mappings, as shown in Figures 4.7(b) and 4.8(b). The white dots in each elemental mapping image indicate the existence and distribution of all the investigated components (Ti, In, O, and Ag) in the photocatalyst samples. It can be clearly seen that all elements of the $0.05In_2O_3$-$0.95TiO_2$ and Ag-loaded $0.05In_2O_3$-$0.95TiO_2$ mixed oxide photocatalysts were well dispersed. The results also imply that the Ag loading by the PCD method provided a high Ag distribution throughout the host mixed oxide. A quantity of each element in the synthesized $0.05In_2O_3$-$0.95TiO_2$ mixed oxide photocatalyst was also

obtained by an analysis of the EDX mapping results, as summarized in Table 4.7. The results show that the number of mole of all components based on 0.95 mol of Ti in the photocatalyst molecular structure was nearly the same as that in its theoretical chemical formula.

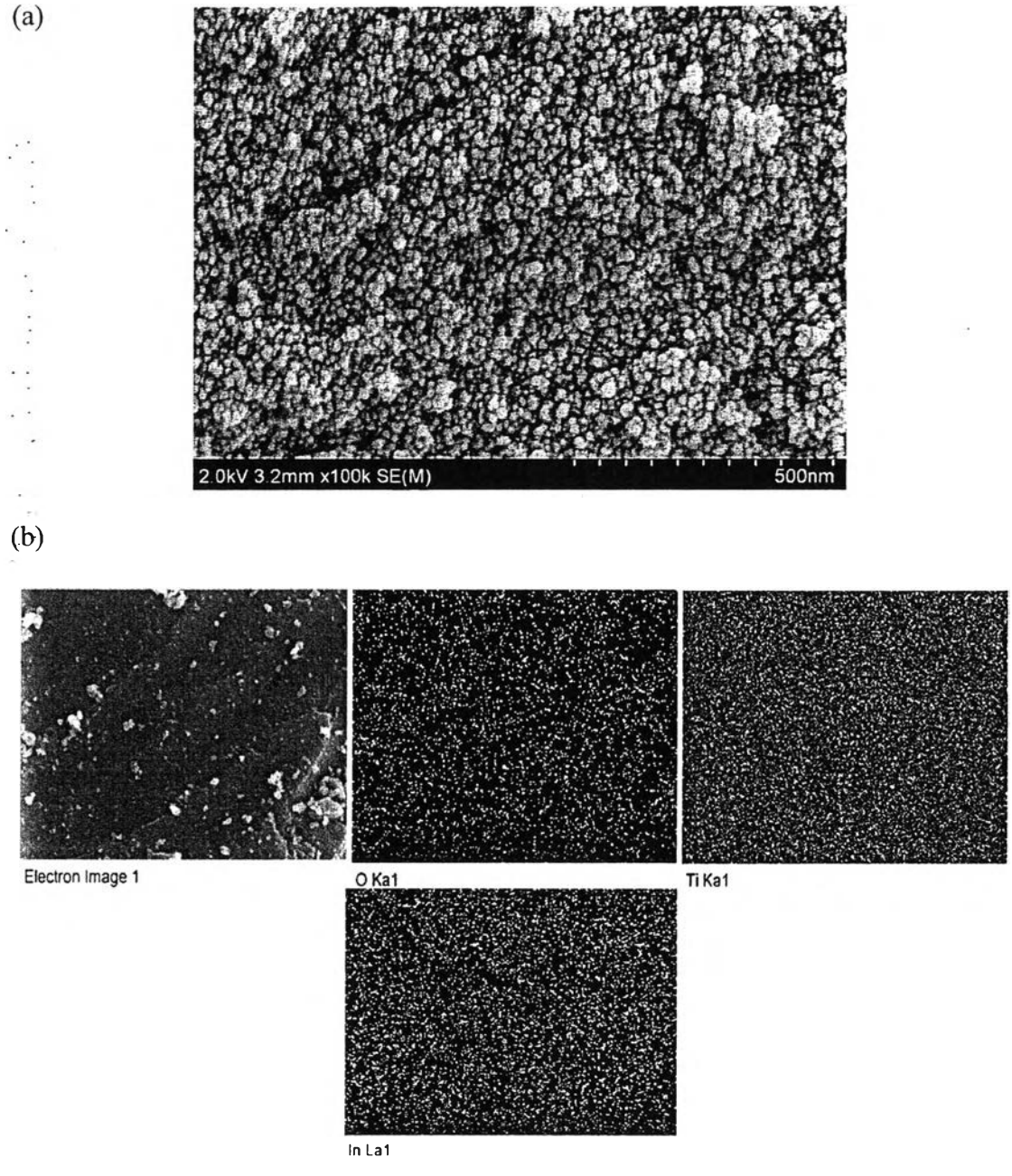

Figure 4.7 (a) SEM image and (b) EDX area mappings of the synthesized mesoporous-assembled $0.05In_2O_3$-$0.95TiO_2$ mixed oxide photocatalyst calcined at 500 °C.

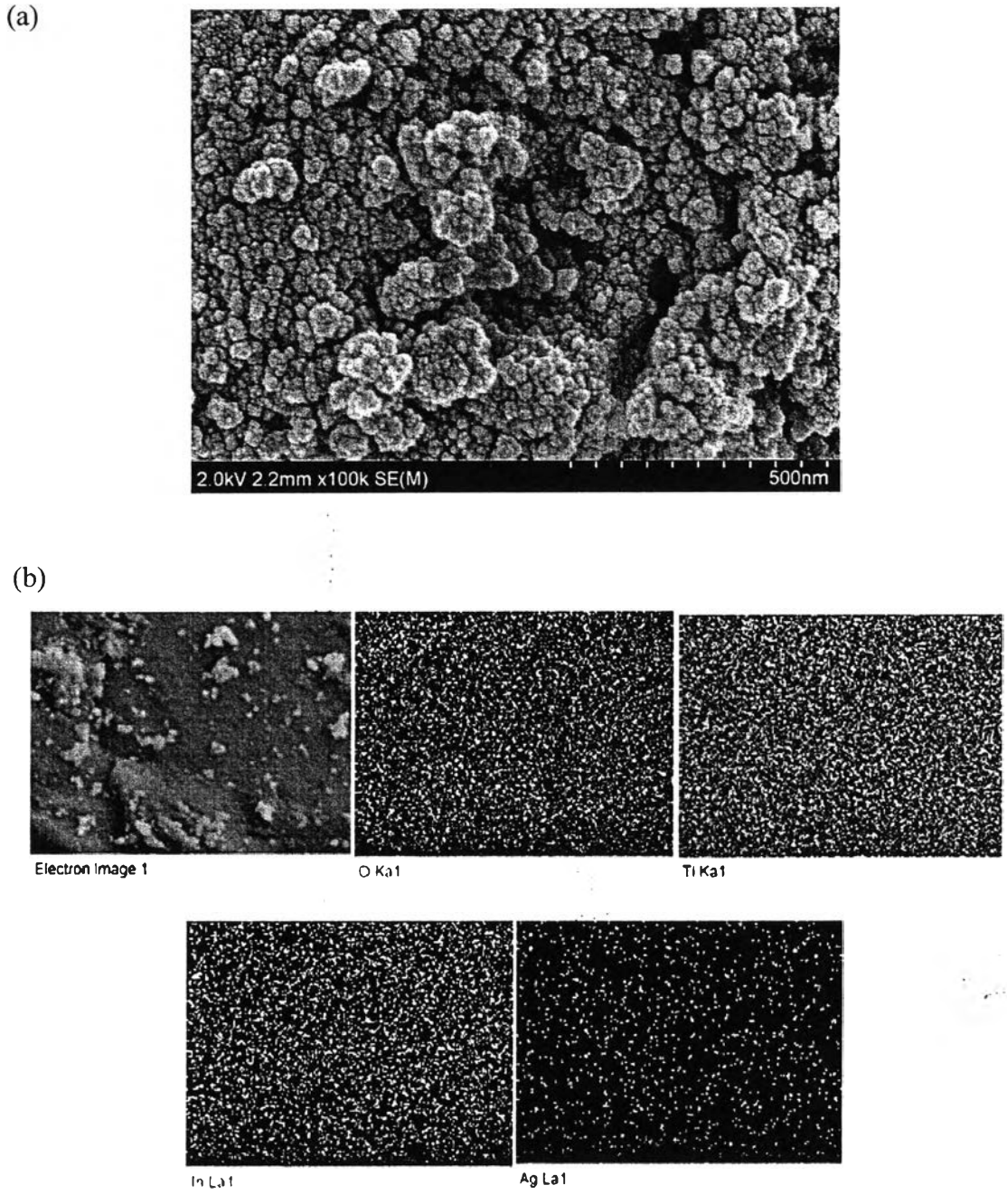

Figure 4.8 (a) SEM image and (b) EDX area mappings of the synthesized 1.5 wt.% Ag-loaded mesoporous-assembled $0.05In_2O_3$-$0.95TiO_2$ mixed oxide photocatalyst calcined at 500 °C.

Table 4.7 EDX mapping results of the synthesized mesoporous-assembled $0.05In_2O_3$-$0.95TiO_2$ mixed oxide photocatalyst calcined at 500 °C

Element	Weight percentage (%)	Molar percentage (%)	Number of mole[(a)]
In	11.57	2.17	0.079
Ti	46.08	26.09	0.950
O	42.35	71.74	2.612

[(a)] Based on 0.95 mol of Ti in the photocatalyst molecular structure

4.1.6 TEM-EDX Results

The morphologies and particle sizes of the synthesized mesoporous-assembled photocatalysts, i.e. the pure TiO_2 calcined at 500 °C and the $0.05In_2O_3$-$0.95TiO_2$ mixed oxide calcined at 500-800 °C, were investigated by the TEM analysis, as illustrated in Figure 4.9. For all the photocatalysts, the aggregation of several nanoparticles was clearly observed, and this confirms the mesoporous-assembled structure of the synthesized photocatalysts, as mentioned above in the SEM results. The average particle sizes of the pure TiO_2 and $0.05In_2O_3$-$0.95TiO_2$ mixed oxide photocatalysts calcined at 500 °C were in the range of 10-15 and 5-10 nm, respectively. A lower particle size of the $0.05In_2O_3$-$0.95TiO_2$ mixed oxide photocatalyst verifies that the incorporation of In_2O_3 to TiO_2 retard the particle crystallization and growth. When considering the $0.05In_2O_3$-$0.95TiO_2$ mixed oxide photocatalyst calcined at different temperatures between 500 and 800 °C, it can be clearly seen that a more severe calcination temperature led to a higher particle growth, as expected. In addition, it was observed that the particle sizes of all the synthesized photocatalysts were similar to the crystallite sizes calculated from the XRD patterns by the Scherrer equation (Table 4.3), indicating a single crystalline characteristic of the samples. Besides, the TEM and EDX mapping analyses of the synthesized 1.5 wt.% Ag-loaded mesoporous-assembled $0.05In_2O_3$-$0.95TiO_2$ mixed oxide photocatalyst calcined at 500 °C was performed. As shown in Figure 4.10, the existence of the Ag nanoparticles on the $0.05In_2O_3$-$0.95TiO_2$ photocatalyst was

clearly observed, as confirmed by the EDX result. The average particle size of the Ag nanoparticles was approximately 5-10 nm.

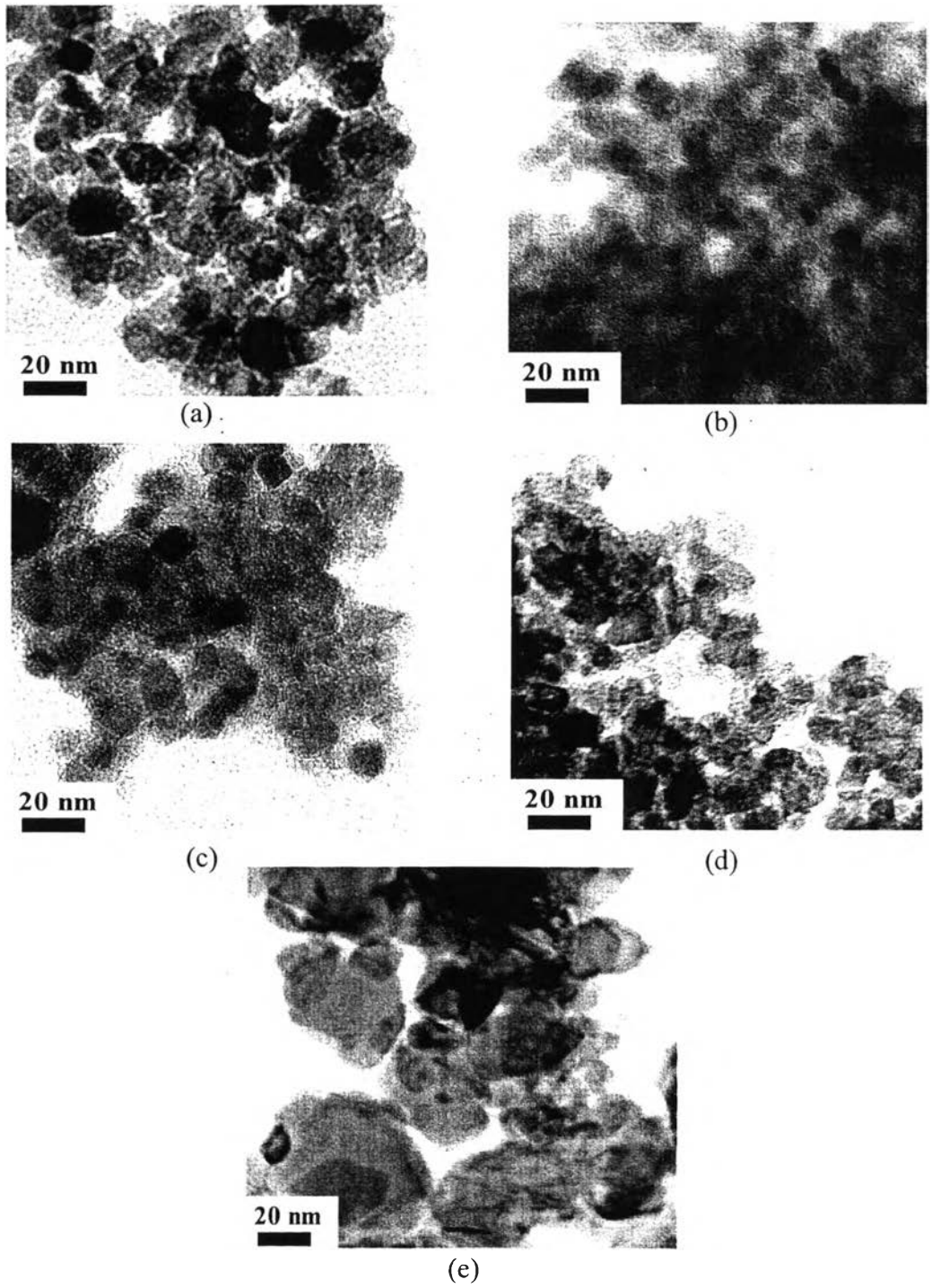

Figure 4.9 TEM images of the synthesized mesoporous-assembled photocatalysts: (a) pure TiO_2 calcined at 500 °C and (b, c, d, and e) $0.05In_2O_3$-$0.95TiO_2$ mixed oxide calcined at 500, 600, 700, and 800 °C, respectively.

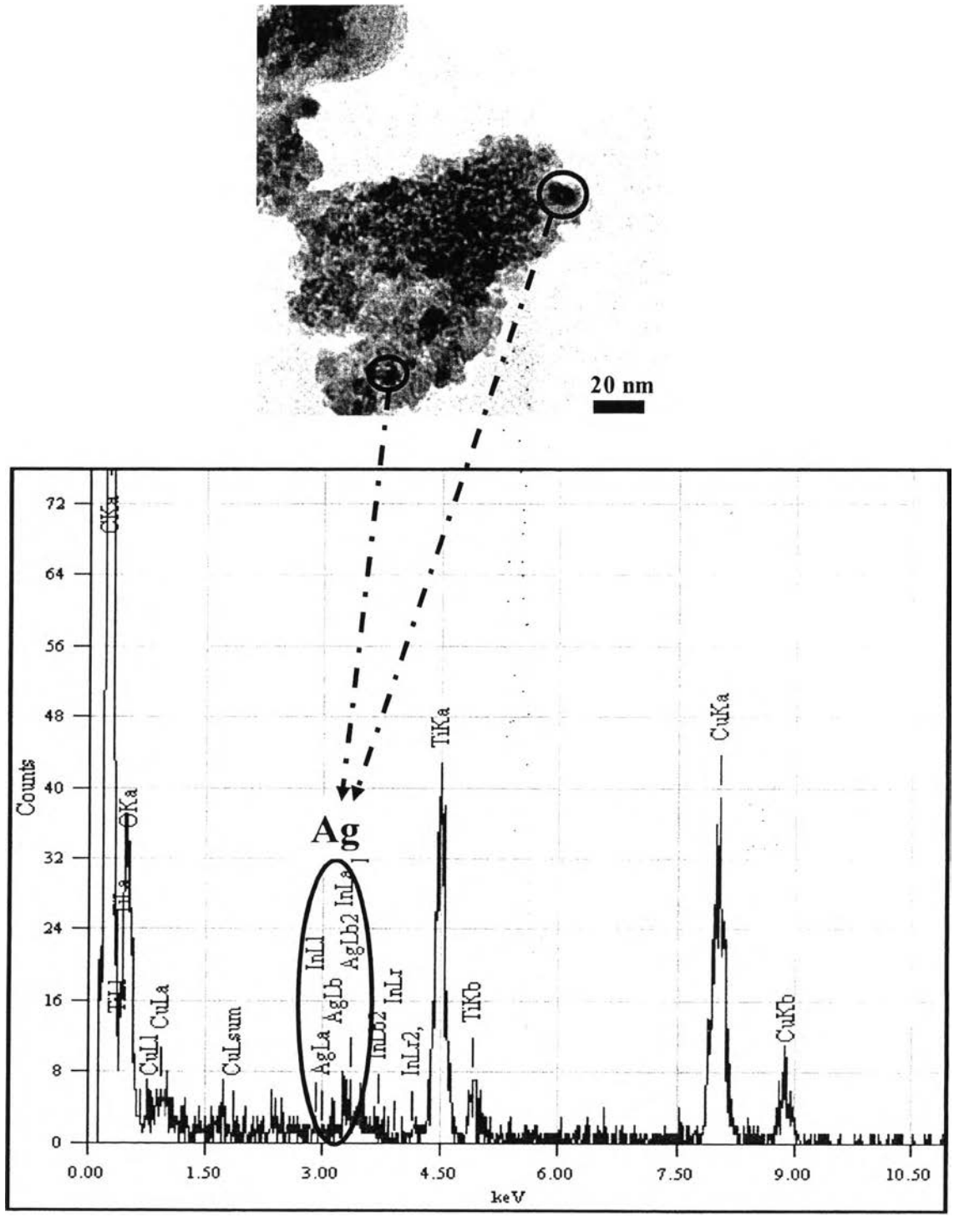

Figure 4.10 TEM image and EDX point mapping of the synthesized 1.5 wt.% Ag-loaded mesoporous-assembled $0.05In_2O_3$-$0.95TiO_2$ mixed oxide photocatalyst calcined at 500 °C.

4.1.7 H_2 Chemisorption Results

The H_2 chemisorption analysis was used to determine the Ag dispersion, as well as the agglomeration of the Ag nanoparticles. The results of Ag dispersion of all Ag-loaded mesoporous-assembled $0.05In_2O_3$-$0.95TiO_2$ mixed oxide photocatalysts are summarized in Table 4.8. It can be seen that the Ag dispersion initially increased with increasing Ag loading to 1.5 wt.%, and then it decreased with further increasing Ag loading up to 2 wt.%. These results imply that the Ag nanoparticle agglomeration occurred at the Ag loadings higher than 1.5 wt.%.

Table 4.8 Ag dispersion results of the synthesized Ag-loaded mesoporous-assembled $0.05In_2O_3$-$0.95TiO_2$ mixed oxide photocatalysts calcined at 500 °C

Ag loading (wt.%)	Ag dispersion (%)
0.5	15.43
1	23.59
1.25	39.31
1.5	62.21
1.75	22.06
2	10.46

4.2 Photocatalytic CR Dye Degradation Results

UV-visible spectroscopy was used to investigate the CR dye degradation performance of the synthesized mesoporous-assembled In_2O_3-TiO_2 mixed oxide photocatalysts without and with Ag loading. The UV-visible spectrum of CR dye solution reveals the maximum absorbance wavelength (λ_{max}) value at 498 nm, as shown in Figure 4.11. This absorbance can be attributed to the $\pi \rightarrow \pi^*$ transition in the azo group (–N=N–) during the light absorption, which represents the color of the CR dye (Sun *et al.*, 2007). Therefore, the decrease in this λ_{max} value was used to evaluate the CR dye degradation performance in terms of decolorization.

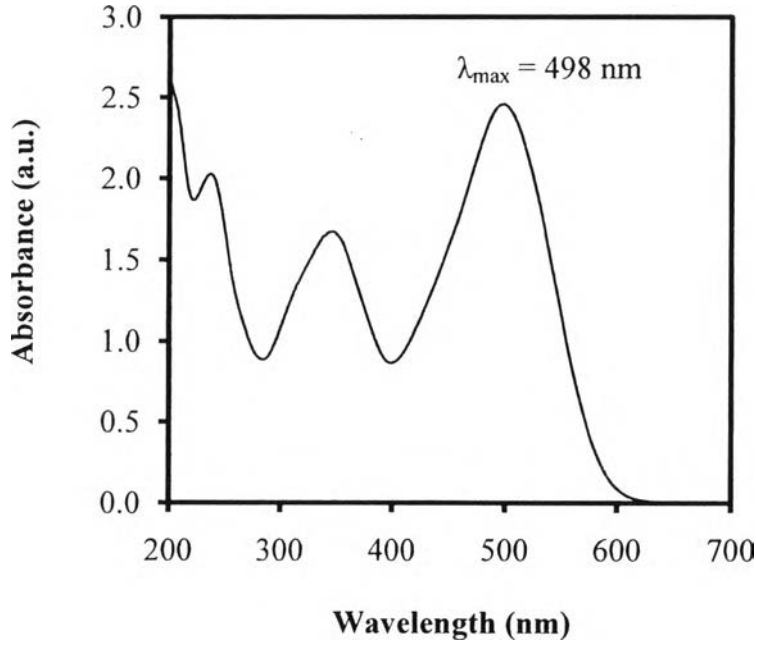

Figure 4.11 UV-visible spectrum of CR dye solution.

4.2.1 Effect of In_2O_3-to-TiO_2 Molar Ratio in Mixed Oxide Photocatalysts

In this research, the mesoporous-assembled In_2O_3-TiO_2 mixed oxide photocatalysts synthesized with various In_2O_3-to-TiO_2 molar ratios calcined at 500 °C were used to investigate the photocatalytic CR dye degradation performance in order to find the suitable In_2O_3-to-TiO_2 molar ratio that exhibits the highest photocatalytic activity. It must be first noted that no appreciable CR dye degradation was detected in the absence of either light irradiation or photocatalyst. The results of reaction rate constant (k) as a function of In_2O_3-to-TiO_2 molar ratio in terms of In_2O_3 content are shown in Figure 4.12. It can be observed that the reaction rate constant significantly increased with increasing In_2O_3 content and reached a maximum value at the In_2O_3 content of 5 mol% (In_2O_3-to-TiO_2 molar ratio of 0.05:0.95). However, it adversely decreased with further increasing In_2O_3 content more than 5 mol%. Therefore, the synthesized mesoporous-assembled $0.05In_2O_3$-$0.95TiO_2$ mixed oxide photocatalyst (with 95 mol% TiO_2 and 5 mol% In_2O_3) provided the highest photocatalytic CR dye degradation activity ($k = 0.86\ h^{-1}$), which was also much higher than that of the commercial P-25 TiO_2 ($k = 0.04\ h^{-1}$). According to the specific surface area analysis (Table 4.1), the incorporation of In_2O_3 enhanced the specific surface area and total pore volume of the In_2O_3-TiO_2 mixed oxide photocatalyst, consequently resulting in more available active sites on the photocatalyst surface, whereas from the XRD results (Figure 4.3 and Table 4.3), the more In_2O_3 incorporation led to a smaller crystallite size and lower crystallinity. However, the band gap energy of the In_2O_3-TiO_2 mixed oxide photocatalysts only slightly increased with more In_2O_3 incorporation; therefore, it might have insignificant role in affecting the photocatalytic activity at the investigated In_2O_3 content of 0-7 mol%. Hence, the higher photocatalytic activity with an increase in the In_2O_3 content up to 5 mol% is possibly because of the higher surface active sites available due to the increases in the specific surface area and pore volume, as well as the lower probability of charge carrier recombination at the bulk traps due to the decrease in the crystallite size. Even though the decrease in the crystallinity was observed, its negative effect might not exceed the positive effects of the specific surface area, total pore volume, and crystallite size in improving the photocatalytic activity in the In_2O_3 content range of 0-5 mol%. However, the observed decrease in the photocatalytic

activity with the further increase in the In_2O_3 content higher than 5 mol% can be explained by the combination of very small crystallite size and very low crystallinity, which might increase the probability of charge carrier recombination at both the surface and bulk traps. Even though the higher specific surface area and total pore volume were obtained a higher In_2O_3 content, their positive effects might not be sufficiently high to enhance the photocatalytic activity. These results indicate that a well-controlled balance among the physicochemical properties is desired by manipulating the In_2O_3 content in the the In_2O_3-TiO_2 mixed oxide photocatalyst in order to achieve the highest photocatalytic activity. In overall, the synthesized mesoporous-assembled $0.05In_2O_3$-$0.95TiO_2$ mixed oxide photocatalyst with a uniform pore size, comparatively high specific surface area and pore volume, and a suitable crystallite size could facilitate the electron and hole transport for reacting with water and/or oxygen molecules adsorbed on its surface along the mesoporous-assembled structure to generate many active species, such as $O_2^{\bullet-}$, $OH^{\bullet}$, and $OH_2^{\bullet}$, for the photocatalytic CR dye degradation. Therefore, the synthesized mesoporous-assembled $0.05In_2O_3$-$0.95TiO_2$ mixed oxide photocatalyst was selected for further experiments to investigate the effect of calcination temperature.

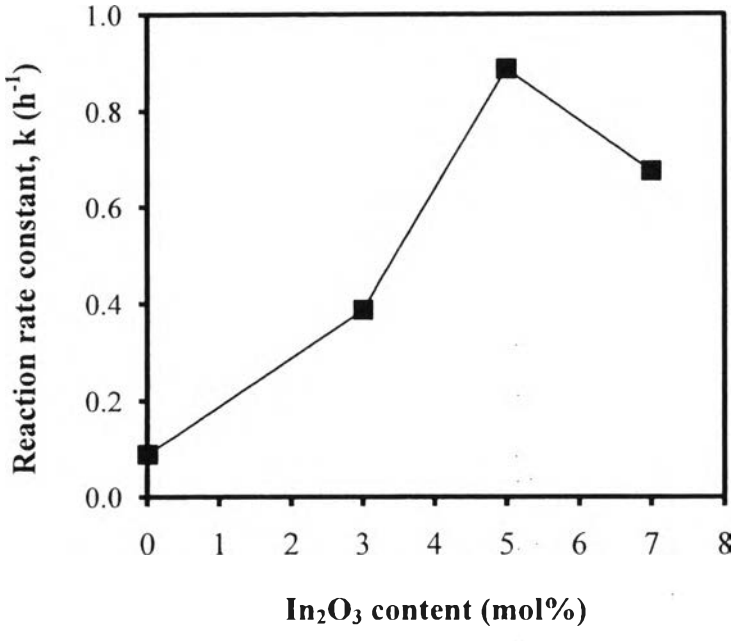

Figure 4.12 Effect of In_2O_3-to-TiO_2 molar ratio in terms of In_2O_3 content of the synthesized mesoporous-assembled In_2O_3-TiO_2 mixed oxide photocatalysts calcined at 500 °C on the reaction rate constant for CR dye degradation (Photocatalyst, 0.5 g; total reaction mixture volume, 100 ml; initial CR dye concentration, 200 mg/l; initial solution pH, 7.04; and irradiation time, 4 h).

4.2.2 Effect of Calcination Temperature

The effect of calcination temperature of the synthesized mesoporous-assembled $0.05In_2O_3$-$0.95TiO_2$ mixed oxide photocatalyst on the photocatalytic CR dye degradation was next investigated. The photocatalytic activity results of the $0.05In_2O_3$-$0.95TiO_2$ mixed oxide photocatalyst as compared to the pure TiO_2 photocatalyst calcined at various temperatures between 500 and 800 °C are shown in Figure 4.13. It was found that the reaction rate constants of both the $0.05In_2O_3$-$0.95TiO_2$ mixed oxide and pure TiO_2 photocatalysts decreased with increasing calcination temperature. These results indicated that the calcination temperature strongly affected the photocatalytic activity of CR dye degradation. These can be explained by the physicochemical properties of the photocatalysts, which were directly governed by the calcination temperature. Even though the higher

crystallinity (Figure 4.4) and the lower band gap energy (Table 4.5) were obtained at a higher calcination temperature, the significant decreases in the specific surface area and the total pore volume (Table 4.1) and the large increase in the crystallite size (Table 4.3) might have more negative influence on the photocatalytic activity by both drastically decreasing the accessibility of the reactant molecules to the surface active sites and increasing the probability of the charge carrier recombination at the bulk traps. In addition, the anatase-to-rutile TiO_2 phase transformation at a higher calcination temperature might exert a negative effect on the photocatalytic activity due to the less driving force of the rutile TiO_2 for the transport of generated electrons to generated active species as compared to the anatase TiO_2, partly leading to the decreased photocatalytic activity at a very high calcination temperature.

From the comparative photocatalytic activity tests, the $0.05In_2O_3$-$0.95TiO_2$ mixed oxide photocatalyst provided much significantly higher CR dye degradation performance than the pure TiO_2 photocatalyst over the entire range of investigated calcination temperature. The higher specific surface area, higher total pore volume, lower crystallite size, and delayed anatase-to-rutile TiO_2 phase transformation of the $0.05In_2O_3$-$0.95TiO_2$ mixed oxide photocatalyst might be the possible reasons in achieving a higher photocatalytic activity at a given calcination temperature as compared to the pure TiO_2 photocatalyst. From the overall results, the calcinations temperature of 500 °C provided superior physicochemical properties for the $0.05In_2O_3$-$0.95TiO_2$ mixed oxide photocatalyst; therefore, it was considered as the optimum value to be used in further experiments.

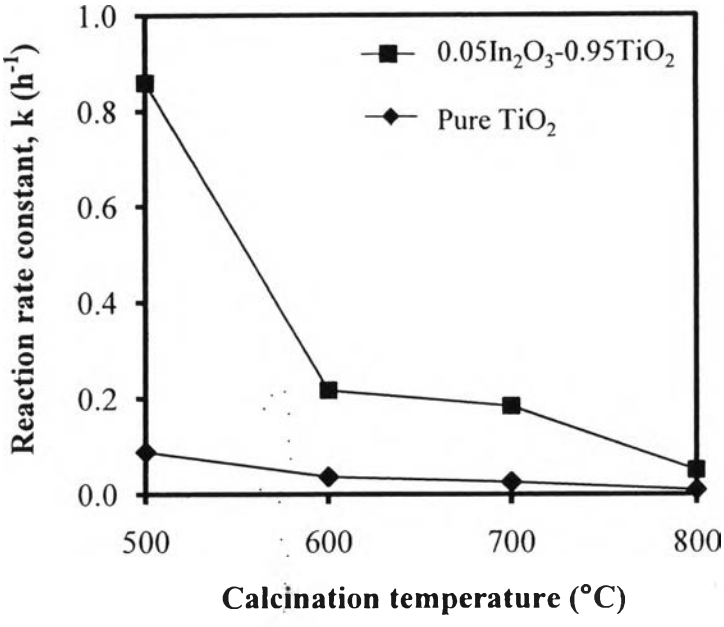

Figure 4.13 Effect of calcination temperature of the synthesized mesoporous-assembled pure TiO_2 and $0.05In_2O_3$-$0.95TiO_2$ mixed oxide photocatalysts on the reaction rate constant for CR dye degradation (Photocatalyst, 0.5 g; total reaction mixture volume, 100 ml; initial CR dye concentration, 200 mg/l; initial solution pH, 7.04; and irradiation time, 4 h).

4.2.3 Effect of Ag Loading

The synthesized mesoporous-assembled $0.05In_2O_3$-$0.95TiO_2$ mixed oxide photocatalyst calcined at 500 °C was used for further investigating the effect of Ag loading in the range of 0.5-2 wt.% prepared by the PCD method on the photocatalytic CR dye degradation. The results of the photocatalytic CR dye degradation in terms of reaction rate constant of the Ag-loaded $0.05In_2O_3$-$0.95TiO_2$ mixed oxide photocatalysts are shown in Figure 4.14. The reaction rate constant increased with increasing Ag loading up to 1.5 wt.%, at which the highest reaction rate constant of 1.36 h^{-1} was observed, and then it adversely decreased with further increasing Ag loading. It was also found that the Ag dispersion increased with increasing Ag loading to 1.5 wt.% and then decreased dramatically with further increasing Ag loading. The results indicate that the Ag dispersion is a prime factor that governs the photocatalytic activity of the Ag-loaded photocatalyst. Therefore, in

the Ag loading range of 0-1.5 wt.%, the highly dispersed Ag nanoparticles loaded on the $0.05In_2O_3$-$0.95TiO_2$ surface could help accelerate the electron transfer and act as an electron sink after band gap excitation in order to prevent the charge carrier recombination. The electrons can accumulate on the Ag nanoparticles and then quickly react with O_2 molecules adsorbed on the photocatalyst surface and/or dissolved in the reaction solution, while the holes can react effectively with H_2O molecules. These suggest that the redox reactions to generate several active species, e.g. $O_2^{\bullet-}$, $OH^{\bullet}$, and $OH_2^{\bullet}$, can occur more easily, resulting in an observed enhancement of the photocatalytic activity. However, for an excessive Ag loading (higher than 1.5 wt.%), the observed decrease in the photocatalytic activity can be explained in that too much Ag loading resulted in higher probability of the Ag nanoparticles to agglomerate and undesirably behave as recombination centers, and this consequently led to a marked increase in the charge carrier recombination frequency because the average distance between trapping sites decreases by increasing the number and the size of Ag nanoparticles confined within a photocatalyst particle (Sreethawong *et al.*, 2006). In overall, the optimum Ag loading for the present investigated system was considered to be 1.5 wt.%.

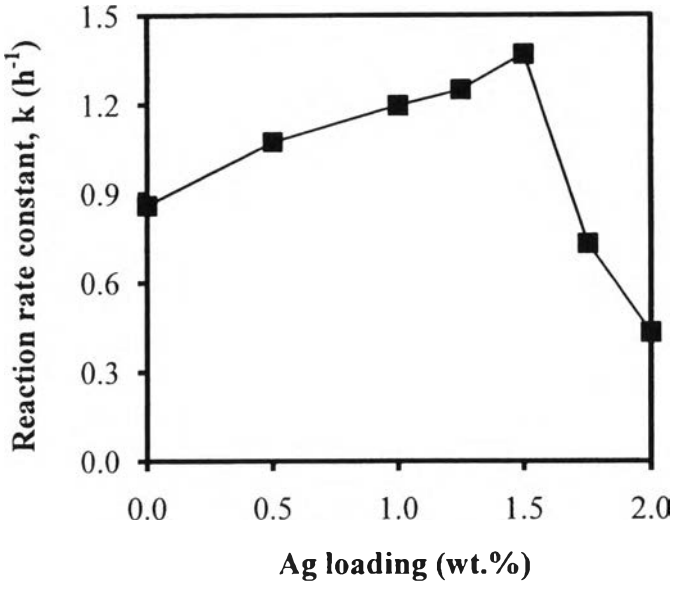

Figure 4.14 Effect of Ag loading on the synthesized mesoporous-assembled $0.05In_2O_3$-$0.95TiO_2$ mixed oxide photocatalyst calcined at 500 °C on the reaction rate constant for CR dye degradation (Photocatalyst, 0.5 g; total reaction mixture volume, 100 ml; initial CR dye concentration, 200 mg/l; initial solution pH, 7.04; and irradiation time, 4 h).

4.2.4 Effect of Water Hardness

The presence of water hardness, as a part of natural organic matters, has been a problem in the many industries due to their water-soluble property and non-biodegradability. Hardness is generally referred to calcium and magnesium present in water with a typical Ca-to-Mg ratio of 3:2, and the normal total hardness concentration is about 120-240 mg/l (Tanthakit *et al.*, 2009). For the photocatalytic activity tests in this work, two different types of water hardness, i.e. pure Ca and mixture of Ca and Mg (Ca-to-Mg ratio of 3:2), were investigated with different total concentrations of 200 and 500 mg/l. The hardness concentration of 500 mg/l was used in the experiments to represent the extremely hard water. The photocatalytic activity results over the 1.5 wt.% Ag-loaded mesoporous-assembled $0.05In_2O_3$-$0.95TiO_2$ mixed oxide photocatalyst calcined at 500 °C in the presence of water hardness are shown in Figures 4.15. The results clearly indicate that the reaction rate

constant significantly decreased with increasing hardness concentration. In addition, it could be observed that the mixture of Ca and Mg more negatively affected the photocatalytic degradation efficiency as compared to the pure Ca at the extremely high hardness concentration of 500 mg/l. The results indicate that the competitive adsorption between dye and hardness molecules played a significant role on the photocatalytic degradation, since the photocatalytic reaction mainly occurred on the photocatalyst surface, but not in the bulk solution (Li *et al.*, 2002). When the hardness was present in the solution, the net positive charge in the solution was dramatically increased due to the positive cation of the hardness molecules. This led to an obstruction of the negatively charged CR dye molecules to adsorb on the photocatalyst surface because of their preferable interaction with the positively charged cations. Particularly, since the Mg cation has a smaller ionic radius than the Ca cation, the Mg cation more easily interacted with the dye molecules as compared to the Ca cation. This caused the dye molecules to approach the photocatalyst surface more difficult, resulting in the observed drastic decrease in the photocatalytic activity. Therefore, the total hardness concentration of 500 mg/l of the mixture of Ca and Mg, which led to the lowest photocatalytic activity, was chosen to further enhance the photocatalytic degradation efficiency by solution pH adjustment.

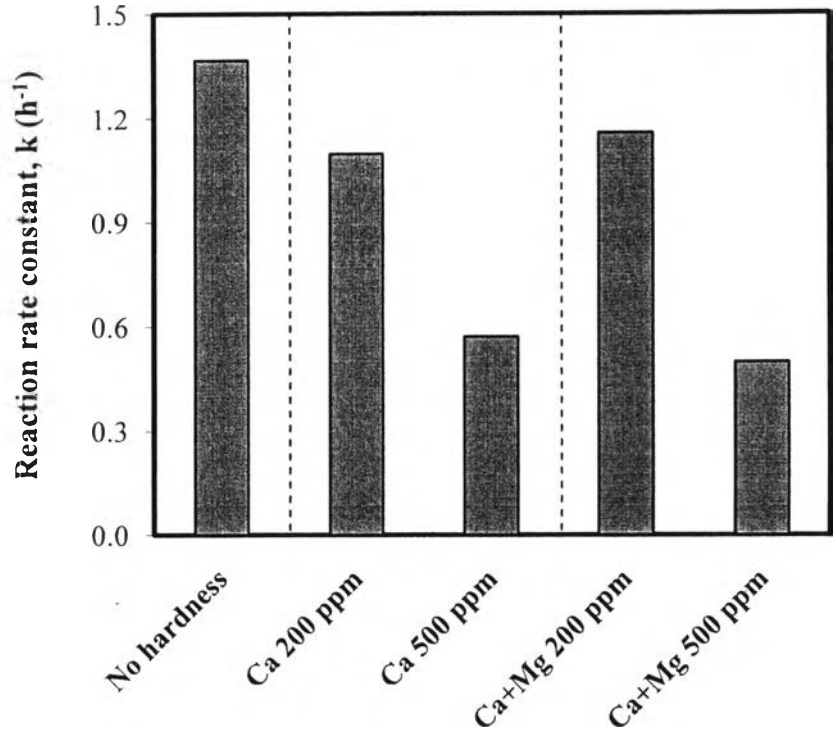

Figure 4.15 Effect of water hardness type and concentration on reaction rate constant for CR dye degradation over the synthesized 1.5 wt.% Ag-loaded mesoporous-assembled $0.05In_2O_3$-$0.95TiO_2$ mixed oxide photocatalyst calcined at 500 °C (Photocatalyst, 0.5 g; total reaction mixture volume, 100 ml; initial CR dye concentration, 200 mg/l; initial solution pH, 7±0.2; and irradiation time, 4 h).

4.2.5 Effect of Initial Solution pH

The pH of solution is an important parameter in the photocatalytic processes, since it not only plays an important role on the characteristics of wastewater but also determines the surface charge properties of a photocatalyst, the charge of dye molecules, the dye adsorption on photocatalyst surface, and the concentration of hydroxyl radicals. In this work, HCl was used to adjust the initial pH of CR dye solution, containing hardness concentration of 500 mg/l in the form of the mixture of Ca and Mg, in the range of 4-7 prior to the photocatalytic activity tests. Figure 4.16 shows the photocatalytic CR dye degradation results over the 1.5 wt.% Ag-loaded mesoporous-assembled $0.05In_2O_3$-$0.95TiO_2$ mixed oxide photocatalyst calcined at 500 °C at various initial solution pHs. The results reveal that the adjustment of the initial solution pH from the original initial solution pH of 7.14

to 5.03 improved the photocatalytic activity. Particularly, a much higher photocatalytic activity was obtained at an initial solution pH lower than the point of zero charge (pzc) of TiO_2 (the main component in the $0.05In_2O_3$-$0.95TiO_2$ mixed oxide), which is about 6.0±0.3 (Parks, 1965). When the CR dye was dissolved in the aqueous solution, its structure became negatively charged; however, the photocatalyst surface became more positively charged when the initial solution pH was lower than its pzc. Hence, these opposite charges favorably led to the enhancement of the photocatalytic activity due to their increased interaction. In the presence of water hardness, the decrease in the initial solution pH could result in the more positively charged photocatalyst surface; therefore, this helped regain the interaction between the dye molecules and photocatalyst surface to achieve a higher photocatalytic degradation activity. However, at too low initial solution pH of 4.05 with the excess concentration of H^+, the H^+ ions tend to interact with the azo link (–N=N–), at which can preferentially be electrophilically attacked by hydroxyl radicals, leading to decreasing the electron densities at the azo group. Consequently, the reactivity of hydroxyl radicals to attack the dye molecules by electrophilic mechanism unfavorably decreases (Sun *et al.*, 2007), resulting in the observed low photocatalytic degradation activity. It can therefore be concluded that the initial solution pH adjustment to a proper value could be employed to enhance the photocatalytic CR dye degradation in the presence of water hardness.

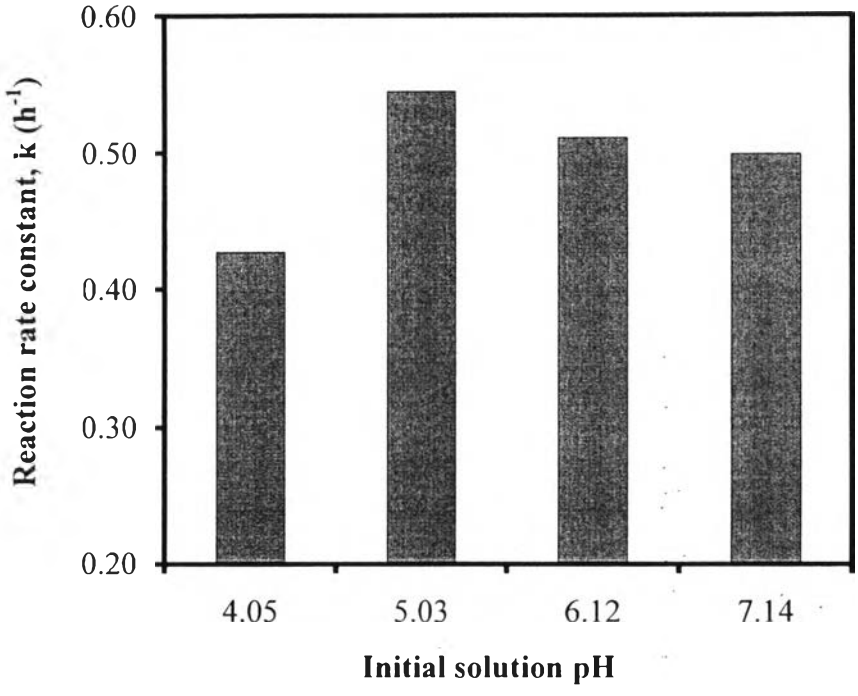

Figure 4.16 Effect of initial solution pH on reaction rate constant for CR dye degradation over the synthesized 1.5 wt.% Ag-loaded mesoporous-assembled $0.05In_2O_3$-$0.95TiO_2$ mixed oxide photocatalyst calcined at 500 °C (Photocatalyst, 0.5 g; total reaction mixture volume, 100 ml; initial CR dye concentration, 200 mg/l; and irradiation time, 4 h).